Analysis of the hysteresis loops of a martensitic steel. Part I and Part II

Benjamin Fournier, Maxime Sauzay, Christel Caës, Michel Mottot, Michel Noblecourt, André Pineau

Analysis of the hysteresis loops of a martensitic steel.
Part II : Study of the influence of creep and stress relaxation hold times on cyclic behaviour.

B. Fournier [a,b,*], M. Sauzay [a], C. Caës [a], M. Mottot [a], M. Noblecourt [a], A. Pineau [b],

[a] *CEA/DEN/DMN/SRMA, Bat. 455, 91191 Gif-sur-Yvette Cedex, France*

[b] *ENSMP, Centre des Matériaux P.-M. Fourt, UMR CNRS 7633, BP 87, 91003 Evry, France.*

Abstract

This second part is devoted to the study of hold time effects on the cyclic plastic behaviour of a martensitic steel tested at 823K. The enhanced stress partitioning method presented in the first part [1] is used to evaluate the kinematic, isotropic and viscous parts of the cyclic stress. Both relaxation and creep hold times of various durations were tested. The bulk Young modulus is found to vary significantly during cycling for creep-fatigue tests, which might be correlated to specific environmental interaction. The viscous stress measured at the end of the hold period tends to vanish as the hold time increases. The introduction of creep hold times enabled to reach higher viscoplastic strains per cycle and to study a larger range of strain rates. In all tested cases the observed softening effect is mainly due to the kinematic stress decrease. Nevertheless if the kinematic stress is always found to decrease with increasing cumulated viscoplastic strain, the initial magnitude of the creep-fatigue kinematic stress (measured at the end of the first hold period) can be either higher or lower than that of the corresponding pure-fatigue test. These effects of the hold period on the kinematic stress value can be linked to the viscoplastic strain rate (and to the nature of the hold: creep or relaxation), the corresponding dependency presents a maximum suggesting that two competing microstructural mechanisms controls the magnitude of the kinematic stress. The enhanced stress partitioning method also enables to evaluate the activation volume of both the creep and fatigue deformation mechanisms. The observed values are compared to those found in the literature.

Key words: Work-softening, kinematic stress, stress partition, martensitic steel, Statistical Process Control, viscosity, high temperature, 9% chromium steel, hold time, creep, relaxation, fatigue.

1 Introduction.

As mentionned in the first part [1], in advanced power generation applications, the 9-12%Cr martensitic steels will be submitted to cyclic loading including hold periods. For pure fatigue loadings, the enhanced stress partionning method presented in the first part [1] enabled to correlate the cyclic softening effect to the decrease of the backstress (X). In addition to the abundant evidence of softening effect in pure fatigue loadings at high temperatures [2–9], this loss of mechanical resistance of martensitic steels has also been reported at lower temperatures [3,10,11], for complex thermomechanical loadings [5,12] and at various stress ratios ($R = \frac{\sigma_{min}}{\sigma_{max}}$) [10,13,14]. Surprisingly enough, even though numerous studies have been dedicated to creep-fatigue interactions [14–24] or cyclic creep loadings [25,26], most of them are focussed on damage accumulation procedures and lifetime predictions. Only very few studies precisely tackle the microstructural variations occurring during creep-fatigue tests [14,22,27,28] and their influence on the mechanical behaviour of 9%Cr steels . Therefore, if the general features of creep-fatigue interactions in terms of damage [29,30] are relatively well documented for these steels, to the authors knowledge, no detailed deformation mechanism map, often drawn from such creep-fatigue tests [31,32], exist for the 9%Cr steels family.
Moreover the creep properties of these steels were extensively studied [27,33–39] and several semi-empirical models, based on the prediction of the microstructural coarsening [28,40–45], were developped to account for the creep behaviour of the 9-12%Cr martensitic steels. However, until very recently [46,47], no model based on microplasticity mechanisms, such as those identified by TEM (Transmission Electron Microscopy) examination combined to stress partition (e.g. for 316 austenitic steel [48]), was available for the description and prediction of their (creep-)fatigue mechanical behaviour. Therefore, the aim of the study is to experimentally quantify the variations of the three stress components (X, R, σ_v) of a 9%Cr martensitic steel submitted to non symmetric cyclic loadings and to relate them to microstructural deformation mechanisms. The present article thus details the study of the cyclic hysteresis loops of creep-fatigue (noted CF) and relaxation-fatigue (noted RF) tests carried either under tensile or compressive hold periods for a wide range of hold times and cyclic strain amplitudes. Firstly, after introducing the experimental conditions, the CF tests results are presented. Such tests where the stress is kept constant (at peak stress), whereas the fatigue cycle is under strain control have been scarcely reported in the literature. Nevertheless, these tests enable to reach higher viscoplastic strains per cycle than usual RF tests and to study a wider range of viscoplastic strain rates. In a second time, the results of the RF tests are discussed. In both cases the variations cycle by cycle of

* Corresponding author.
Email address: benjamin.fournier@cea.fr (B. Fournier).

the isotropic (R), kinematic (X) and viscous (σ_v) stresses are detailed. The last part is dedicated to the link between the microstructural TEM observations and the mechanical results. An attempt is made to propose possible deformation micromechanisms to account for the tests results.

2 Experiments

The material and specimen are identical to these of the pure fatigue tests presented in the first part [1]. As previously mentionned the tests are carried out under total strain control. Nevertheless, for the hold time periods, either the total strain (RF test) or the stress (CF test) are held constant at peak tensile strain. Some results with a compressive hold time are also presented. Thanks to a numerical system, the tensile and compressive stress peaks are continuously recorded. Stress-strain hysteresis loops and stress relaxation curves during hold time were recorded and led to the schematic shown in figure 1.

[Fig. 1 about here.]

All the tests are carried at 823K. For CF tests, the maximum stress is held constant until a given creep strain ϵ_{creep} is reached. For RF tests the hold period is stopped at a given duration. Tables 1 and 2 present the different fatigue strain ranges and tensile holds tested in addition to the relaxed stress measured at half life $\left(\frac{N_f}{2}\right)$ for RF tests.

[Table 1 about here.]

[Table 2 about here.]

Additionally to these CF and RF tests, four sequential tests are carried out at 823K and $\Delta\epsilon_{fat} = 0.7\%$. During these four pure-fatigue tests a single long relaxation (fifteen days) is applied either after the first loading or after the 500^{th} cycle. All the other cycles are pure-fatigue strain controlled ones. These tests were carried out in order to obtain additional information about the interaction between relaxation and cycling and their respective influence on the mechanical behaviour.

3 Results

In the following graphs the variations of the kinematic, isotropic and viscous parts of the cyclic stress are not plotted in terms of number of fatigue cycle,

but in terms of cumulated viscoplastic strain. Indeed, these plots facilitate the comparison of the different results and their interpretation in terms of the physical mechanisms responsible for (visco)plastic deformation, and they are very often used in fatigue and micromechanical modeling [49–51]. Additionally, the observations of the head of the specimens [46] showed that no significant microstructural change occurred due to the effect of aging. Therefore, the results were not plotted in terms of time, but in terms of cumulated viscoplastic strain.

3.1 Cyclic creep tests.

3.1.1 Variation of the stress range ($\frac{\Delta\sigma}{2}$)

In order to illustrate the global variation of the shapes of the CF hysteresis loops, figure 2 presents four hysteresis loops recorded at the 1^{st}, 100^{th}, 750^{th} and 875^{th} cycles for a CF test carried out at a fatigue strain range $\Delta\epsilon_{fat} = 1\%$ and a creep strain $\epsilon_{creep} = 0.5\%$. As in the case of pure fatigue tests a significant softening effect of the steel is observed during cycling. The viscoplastic strain range increases slightly during cycling since the tests are controlled on total strain. This figure also reveals that, between the 750^{th} and the 875^{th} cycles macroscopic damage has appeared and developped since the compressive half loop of the 875^{th} is strongly distorted.

[Fig. 2 about here.]

In CF tests, due to the hold period, the strain interval is not symmetrical anymore, since the total strain varies between $-\frac{\Delta\epsilon_{fat}}{2}$ and $\frac{\Delta\epsilon_{fat}}{2} + \epsilon_{creep}$. This non symmetrical loading results in the existence of a compressive mean stress (since the hold period is in tension). Indeed since the additional viscoplastic creep strain must be erased during the compressive half loop, the magnitude of the peak compressive stress is larger than that of the maximum tensile stress. Figure 2 presents variations of the measured mean stress values for a pure fatigue and CF tests carried out at the same $\Delta\epsilon_{fat}$ and various creep strains. In the case of a pure fatigue test ($\epsilon_{creep} = 0$), a slightly positive mean stress ($\sigma_{mean} \leq 10$MPa) exists. As expected, the magnitude of the compressive mean stress increases (up to $55MPa$ in some cases) as the imposed creep strain ϵ_{creep} and the cumulated viscoplastic strain ϵ^{vp}_{cum} increase for CF tests. This figure presents also the mean stress obtained for a compressive hold CF test, and it turns out to be also opposite to the hold sign, even though its magnitude is relatively lower than that of the corresponding tensile hold CF test.

As noted in figure 2, a significant softening effect is also measurable under CF loading. The main question arising is thus : *"do the interactions between fatigue and creep straining modify the softening rate or amplitude?"*. Figure 3.a shows that for high fatigue strain range ($\Delta\epsilon_{fat} = 1\%$) whatever the applied creep strain, the stress range $\frac{\Delta\sigma}{2}$ lays on the same curve when plotted in terms of cumulated viscoplastic strain ϵ^{vp}_{cum} defined as :

$$\epsilon^{vp}_{cum}(N) = 2\sum_{i=1}^{N} \Delta\epsilon^{vp}(i) \tag{1}$$

where $\Delta\epsilon^{vp}(i)$ is the viscoplastic strain experienced by the sample during cycle i.

This result may mean that there is no difference in the softening mechanism between fatigue and CF loadings at high strain range. Nevertheless, when studying the peak tensile stress, this uniqueness of the softening rates does not hold anymore, and the higher the applied creep strain is, the stronger and the faster the softening is. This discrepancy between tensile peak stress and stress range variations might seem surprising. However as for the existence of a compressive mean stress, it is linked to the fact that, in compression, the additional ϵ_{creep} must be erased during load reversal.
For lower fatigue strain ranges, even the stress range $\frac{\Delta\sigma}{2}$ decreases faster when a creep strain is applied, suggesting that CF and fatigue softening effects may proceed from different mechanisms. No trivial conclusion can be drawn from these apparently contradictory results, and they will be discussed further below.

[Fig. 3 about here.]

3.1.2 Variation of the isotropic stress (R)

The variations of the isotropic stress for CF tests are almost identical, whatever the fatigue strain range $\Delta\epsilon_{fat}$. Figure 4 presents those obtained for $\Delta\epsilon_{fat} = 0.7\%$. Both the compressive and tensile isotropic stresses are plotted. In tension, the isotropic stress is completely insensitive to the presence or not of a hold period and, as in the pure fatigue case, it does not decrease (or only very slightly) during cycling, except at the very end of the test. However the corresponding results are biased by the presence of a macroscopic crack in the specimen. The compressive isotropic stress appears to be continuously lower than the pure fatigue one even though it only decreases slightly.

[Fig. 4 about here.]

3.1.3 Variation of the kinematic stress (X)

As a general feature of fine and ultra-fine grained alloys (e.g. low carbon steels [52], Copper and Aluminium alloys [53,54], or even nanocrystalline materials [55]) the backstress is known to be a major part of the cyclic stress. In pure fatigue tests, the first part of this work [1] led to the conclusion that the cyclic softening effect was mainly linked to the decrease of the kinematic part of the cyclic stress X. Figures 5 a) to f) present the variation of both the compressive and tensile kinematic stresses for $\Delta\epsilon_{fat}$ respectively equal to 1%, 0.5% and 0.4% and various applied creep strains. In all cases, in compression, X is higher for CF tests than for pure fatigue ones. Whereas for $\Delta\epsilon_{fat}$ equal to 1% and 0.5% the cyclic decrease of X in compression is comparable for fatigue and CF tests and the amount of applied creep strain does not play a significant role (at least for $\epsilon_{creep} \geq 0.1\%$). This does not hold anymore for the lowest fatigue strain range (see figure 5 e), since on the one hand X decreases faster when the applied creep strain increases. On the other hand in the pure fatigue test, X remains almost constant during the first cycles which is not true for the CF tests.
In tension, the influence of creep periods on the kinematic stress value depends on the fatigue strain range applied. Indeed, as shown in figure 5.b, for $\Delta\epsilon_{fat} = 1\%$, the CF kinematic stress is always 100MPa higher than the pure fatigue one. The applied creep strain leads thus to a strong increase of X. For an intermediate fatigue strain range ($\Delta\epsilon_{fat} = 0.5\%$), applying a creep strain of 0.1% increases X by approximately 50MPa, whereas higher creep strains lead to a kinematic stress appreciably equals to that of the pure fatigue test. Finally for the lowest tested fatigue strain range ($\Delta\epsilon_{fat} = 0.4\%$), the kinematic stress measured at a given ϵ_{cum}^{vp} is found to be smaller when applying a creep period.
In addition, for $\Delta\epsilon_{fat} = 0.5\%$ and 0.4%, the kinematic stress of pure fatigue tests presents a kind of latency phase, during which it remains almost constant before decreasing. In no CF test this delayed decrease of X has been measured since X immediately decreases after the first cycle. These results suggest a complex dependency between X and the applied creep strain. Several competing mechanisms and phenomena may thus be implied in the kinematic stress variations. Exploratory explanations will be proposed in the discussion below.

[Fig. 5 about here.]

The influence of the fatigue strain range on X in CF tests is also illustrated in figure 6 where the variations of the kinematic stress are plotted for a given applied creep strain at various fatigue strain ranges. As expected the kinematic stress amplitude increases with the applied fatigue strain for a given ϵ_{cum}^{vp}. Moreover it can be noticed that the higher the fatigue strain range is,

the faster X decreases. Here again this suggests that the fatigue strain range or an associated parameter plays a major role in the variations of the kinematic stress under CF loadings.

Additionally, figures 5 and 6 show that, whatever the testing conditions, the kinematic stress decrease can be satisfactorily described by a logarithmic relationship: $X = a.log(\epsilon_{cum}^{vp}) + c$ (with a and c depending on the test) before macroscopic damage leads to an abrupt fall of X.

[Fig. 6 about here.]

3.1.4 Variation of the viscous stress (σ_v)

As highlighted for pure fatigue tests, studied in the first part [1] of this work, and mentionned in the literature, viscosity is one of the main mechanisms controlling the deformation of martensitic steels, especially for temperature above 673K [10,12,56]. This effect has already been taken into account in cyclic ratchetting modeling of 9%Cr steels [57]. Figure 7 shows the variation of the viscous stress σ_v for CF tests with various tensile holds and $\Delta\epsilon_{fat} = 1\%$. In compression the viscous stress is virtually insensitive to the addition of a hold period in tension. On the contrary, in tension, the viscous stress, measured at the end of the hold period, is severely reduced by the application of a creep hold. As expected, due to the decrease of the straining rate, the viscous stress that was initially around 130MPa in pure fatigue falls down to 50 and 35MPa respectively for $\epsilon_{creep} = 0.1\%$ and 0.2%. For higher applied creep strain the viscous stress is negligible. Additionally, the results obtained for smaller fatigue strain ranges show that, as soon as $\epsilon_{creep} = 0.1\%$ the viscous stress can be considered as almost null. Therefore, it appears that, when a creep strain is applied, the viscous stress, that reached up to one third of the total pure fatigue stress, decreases very rapidly.

[Fig. 7 about here.]

Such a decrease might have been expected since the viscous stress is linked to the straining rate and their relationship is often expressed in the following way :

$$\dot{\epsilon}^{vp} = \dot{\epsilon}_0^{vp} \times exp\left(-\frac{Q - V^*\sigma_v}{kT}\right) \tag{2}$$

$$\dot{\epsilon}^{vp} = \dot{\epsilon}_0^{vp} \times exp\left(\frac{-Q}{kT}\right) \times exp\left(\frac{V^*\sigma_v}{kT}\right) \tag{3}$$

naming α the following quantity $\dot{\epsilon}_0^{vp} \times exp\left(\frac{-Q}{kT}\right)$, this leads to :

$$\dot{\epsilon}^{vp} = \alpha \times exp\left(\frac{V^* \sigma_v}{kT}\right) \qquad \text{with} \quad \alpha \in I\!R \tag{4}$$

with Q is the enthalpy, V^* the activation volume of the straining mechanism, k the Boltzmann constant and T the absolute temperature. Thus, as the creep straining rate is much smaller than that of pure fatigue, the viscous stress is expected to decrease.

3.2 Cyclic and sequential relaxation tests.

3.2.1 Variation of the stress range ($\frac{\Delta\sigma}{2}$)

RF tests and sequential tests were studied in the same way. Figure 8 presents the variation of the stress range $\Delta\sigma/2$ with the cumulated viscoplastic strain for a fatigue strain amplitude $\Delta\epsilon_{fat} = 0.7\%$ and various relaxation times. It appears that the softening effect is faster and starts at the first cycle under RF loading contrary to pure fatigue for which the softening is a little delayed. Nevertheless, there is no difference between 10 and 30 minutes of hold time and for $\epsilon_{cum}^{vp} \simeq 10$, the stress range is approximately equal to that obtained in pure fatigue. The same variations were observed for relaxation holds of 30 and 90 minutes at $\Delta\epsilon_{fat} = 0.6\%$.
For sequential RF tests (pure fatigue tests with one single fifteen days relaxation), no difference exists with the pure fatigue test in the variation of the stress range, whatever the position (1^{st} or 500^{th} cycle) of the 15 days of relaxation.

[Fig. 8 about here.]

3.2.2 Variation of the isotropic stress (R)

Absolutely no influence of relaxation, either in cyclic or sequential tests, was observed on the isotropic stress which is approximately the same than in pure fatigue tests.

3.2.3 Variation of the kinematic stress (X)

[Fig. 9 about here.]

Figure 9 presents the variation of the kinematic stress for the cyclic RF tests. Contrary to the isotropic stress, relaxation significantly lowers the value of the kinematic stress, which is visible already at the first cycle. Here again no matter the duration of the hold (no difference is visible between 10 and 30 minutes). The difference of X between RF and pure fatigue vanishes for high cumulated viscoplastic strains. Such a decrease of the backstress during constant-strain hold periods has already been measured in 2.25%Cr-1Mo steel by Challenger & Vining [58] who linked it to the effective dislocation barrier strength of the carbides that changes during asymmetric loadings.
For the sequential relaxation tests, when the fifteen days relaxation period occurs at the end of the first load, no difference with the pure fatigue X exists, except just after the relaxation. Indeed, the cross in figure 9 represents the kinematic stress measured at the end of the relaxation period. Surprinsingly enough the obtained value is negative ($-18MPa$). When the relaxation period occurs after 500 fatigue cycles, the kinematic stress is also negative ($-30MPa$) just after the relaxation phase. These unexpected and rather unrealistic negative values may be interpreted in two ways. On the one hand, these values should be considered as null, the low number of points available and the precision of the stress partitioning method (evaluated as close to $\pm 15MPa$ in the first article) leading to slightly negative values, whereas the "true" backstress is negligible. On the other hand, the direct use of the Cottrell partition scheme [59–62] should be discussed in the case of hysteresis loops with hold periods. Indeed, the calculation of X, R and σ_v with the following equations :

$$X = \frac{\sigma_e^{max} + \sigma_e^{min}}{2} \tag{5}$$

$$\sigma_v = \sigma_{max} - \sigma_e^{max} \tag{6}$$

$$R = \frac{\sigma_e^{max} - \sigma_e^{min}}{2} \tag{7}$$

is based on the assumption that σ_e^{max} and σ_e^{min} are respectively the tensile and compressive yield stress and $\sigma_{max} \geq \sigma_e^{max}$. Under pure-fatigue loadings this hypothesis is usually verified. Nevertheless, when a hold time (either a creep or relaxation one) is applied the viscoplastic strain rates at the end of this hold period are severely lower than during cycling. Therefore, the fact that the stress at the end of the hold period (noted $\sigma_e^{unloading}$ at point B in figure 10) actually corresponds to the tensile yield stress of the material may be questioned. In order to investigate this point two additional sequential RF tests were carried out. Here again, a fifteen days relaxation period is applied either after the first loading or after the 500^{th} cycle. However, after the relaxation period (point B), instead of simply continuing the cyclic loading, the stress is brought back to zero (point C) and a new pure fatigue test is carried out

(towards point D). This procedure illustrated in figure 10 enables to evaluate the tensile yield stress after relaxation (noted $\sigma_e^{reloading}$).

[Fig. 10 about here.]

The results obtained are gathered in table 3. In both cases the tensile yield stress obtained after reloading is higher than the stress reached at the end of the relaxation time. This leads to higher (and positive) values of both X and R. Such a difference between the actual tensile yield stress and the stress reached at the end of the relaxation may, at least partly, be explained by a pronounced strain rate effect observed at high temperature on these steels. It is illustrated in figure 11, where monotonic tensile tests were carried at various strain rates.

[Table 3 about here.]

[Fig. 11 about here.]

These results imply that, especially for RF tests, but also for CF tests, the values of X and R obtained by the direct application of the Cottrell partition scheme should be considered as underestimated due to the differences in strain rate between the hold period and the cycling one. These underestimates are up to $100MPa$ in RF, whereas for creep fatigue tests, where the creep rate is generally higher (the same order of magnitude as in figure 11), the underestimate is thought to be less pronounced ($\leq 50MPa$).

The results of figure 9 suggest that, even a very long relaxation does not durably modify the microstructural origins of the kinematic stress, since except for the first cycle after relaxation, the following cycles present the same kinematic stress as if there had been no relaxation. Nonetheless, when a relaxation hold is applied at each cycle, the dislocations rearrangements occurring during these hold periods tend to lower X. This particular result (also found in [63]) clearly invalidates one of the usual methods encountered in the literature to evaluate σ_v [64]. In this method a relaxation test is carried out and the viscous stress is measured as the global stress decrease, the stress at the end of the relaxation (when the stress decrease has stopped) being the internal stress. However the present results show that during relaxation the kinematic stress also decreases as already noted by Feaugas [65] and measured by Sauzay [63]. Other methods based on successive short relaxation or creep phases [66–69] evaluate the viscous stress thanks to the assumption that, during relaxation : $\Delta X \ll \Delta(R+\sigma_v)$ [69]. The above results show that, for long hold periods this relationship does not hold anymore, and thus, these methods must be used carefully (very short hold times must be applied).

3.2.4 Variation of the viscous stress (σ_v)

[Fig. 12 about here.]

As far as the viscous stress is concerned, the RF tests lead to its vanishment as in the CF case. Figure 12 presents the viscous stress values for the cyclic RF tests and the sequential ones. For cyclic hold times of 10 and 30 minutes the viscous stress completely vanishes for $\Delta\epsilon_{fat} = 0.7\%$. For sequential tests, when the relaxation period is applied at the first cycle, the viscous stress is null just after it, but finally reaches almost its pure fatigue value (in fact it remains always 20 MPa lower than it) after a given number of cycles (approximately 100). When the hold period is applied after 500^{th} cycles, the number of cycles needed to reach a viscous stress close to the pure fatigue one is a little shorter (approximately 50 cycles).

4 Discussion

The above results supply a large amount of information about the effects of the interactions between hold times and cyclic loadings on the mechanical behaviour of 9-12%Cr martensitic steels. The following part tackles the effect of hold times on the effective Young modulus, and discusses the variations of the three stress components (X, R, and σ_v) before comparing these results to previous modelings.

4.1 Variations of the effective Young modulus.

The enhanced stress partitioning method enables us to evaluate an effective Young modulus during cycling. In pure fatigue it appeared to slightly decrease until an abrupt fall occurs due to macroscopic crack propagation. Surprisingly enough, in CF tests, the effective Young modulus is found to be always initially higher $170 \leq E \leq 180$GPa than that of pure fatigue, and to often increase during cycling as shown in figure 13. Whereas the slight cyclic decrease of the Young modulus might be linked to the coarsening of the subgrains as suggested in the first part [1], no evident microstructural change appears responsible for this cyclic increase in CF and lath coarsening is also observed. Such Young modulus increases may arise from the propagation of a crack outside of the extensometer range, however it was not the case in the results of figure 13.
Nevertheless the observation of tested samples revealed a strong influence of environment on the cracking behaviour of this steel [3,16,70–74]. The observation and the modeling of these interactions are still in progress [70,71] and

numerous studies deal with the specific oxidation kinetics of 9%Cr steels [75–80]. One of the observed features is that, for most CF tests a large number of widely opened secondary cracks existed and were completely filled with a thick oxide layer, whereas in the pure fatigue cases, only very sharp and bifurcated secondary cracks appeared. When several long cracks are filled with oxide, the sample reacts as a kind of lamellar composite material, and the apparent Young modulus is a mixture of the steel and oxide moduli. As the Young moduli of oxides are higher (between 190 and 300 GPa at 823K depending on the nature of the oxide scale formed) than that of the steel [81] the resulting apparent Young modulus is higher than that of the initial steel. This simple scenario may be a partial explanation of the increasing Young modulus measured during CF tests. Finite element calculations will be carried to validate this hypothesis in future work.

[Fig. 13 about here.]

4.2 Effect of hold periods on the isotropic stress R.

The isotropic stress R corresponds to the stress required by a dislocation to move locally [65], and to overcome short range barriers (precipitates, solid solution,...). The previous results showed that the isotropic component R of the tensile cyclic stress is completely insensitive to the presence or not of a hold period in tension. Moreover a qualitative examination of the TEM observations (see figure 17) revealed no visible precipitates coarsening even for the longest test duration (3 months). However, when a tensile creep-hold is applied, the value of R in compression was found to be slightly lower than that of the corresponding pure fatigue test. Even though R is an isotropic component, as the loading is not symmetrical anymore when applying a hold, R has no reason to be equal in tension and compression. Nevertheless it remains surprising that R decreases in compression whereas the peak compressive stress is larger (in absolute value) than the tensile one. This unexpected decrease could be attributed to some recovery process or intergranular stress redistribution, but further investigations must be carried out to confirm this assumption.

4.3 Effect of hold periods on the viscous stress σ_v.

The viscous stress σ_v is related to time and temperature dependent processes, like dislocation climb or cross-slip and intergranular phenomena. It has been found to drastically decrease when hold times are applied. As expected, the decrease of the viscoplastic strain rate which is the driving force of viscosity, led to the vanishing of the viscous stress.

Moreover the result presented in figure 7 can be used to evaluate the activation volume of the viscous glide, using equation 4. When plotting the values of the viscous stress at the end of the first loading (in order to avoid taking into account the possible effect of cycling) in terms of viscoplastic strain rate, one can fit equation 4 on the data. This is done in figure 14 for both pure fatigue and CF loadings (for CF tests, the duration of the creep period is also indicated). The linear regressions lead to activation volumes of about $230b^3$ and $26b^3$ for creep and fatigue deformation, respectively. These results are in accordance with literature since bcc materials are known to have low activation volumes [55] strongly depending on the alloying elements, the temperature and the strain rate [82]. A brief literature survey of activation volumes and activation energies of some steels and iron alloys is presented in table 4, and shows that, depending on the experimental technique used, the temperature and the material, the activation volumes for viscous glide, even though always low, can widely vary. In addition, the activation energies, even though always higher than the self-diffusion energy that is about $250kJ.mol^{-1}$ can also significantly differ.

[Table 4 about here.]

Such small values for the activation volume suggest that the corresponding viscoplasticity is a phenomenon driven by events taking place at a scale much smaller than the thinnest microstructural scale of these steels [83]. Indeed, the subgrain scale and the lath thickness of modified 9Cr-1Mo steel are about 0.5 to 0.8 μm [2,9].
Moreover, figure 7 shows that the value of the viscous stress only slightly varies during cycling which means that whatever the phenomena responsible for the softening effect they do not influence much the viscous glide. This observation is confirmed by the fact that, when plotting the viscous stress values obtained at (e.g.) the 100^{th} and 500^{th} cycles they reasonably fall on the fitted lines of figure 14 (for CF tests, all the points are situated in the shaded region). This highlights the fact that microstructural variations due to cycling do not affect viscous glide that occurs at a much finner scale.

[Fig. 14 about here.]

In order to complete the study of the phenomena involved in the viscous stress decrease during hold time and to evaluate more precisely their activation energy, temperatures around 823K should be explored. As reported in the first article, temperature has a strong effect on the viscous stress magnitude since pure fatigue tests carried out at 673K exhibited a very low viscous stress ($\leq 40MPa$), even for the highest applied strain level. This rapid build up of the viscous stress between 673K and 823K can be related to the deformation-

mechanism maps edited by Frost and Ashby [84]. Indeed, creep deformation and viscous phenomena at 823K can occur easily for bcc materials, whereas for fcc materials (e.g. 316 stainless steel) they only take place for temperature approximately 100°C higher. This observation is compatible with viscous stress measurements carried out by Delobelle [85] and Catalao [86] who showed that σ_v was almost negligible at 823K whereas at 873K it already reached approximately 80MPa for a 316 austenitic steel.

4.4 Effect of hold periods on the kinematic stress X.

Generally speaking the backstress is the directional component of the stress which corresponds to long range interactions with dislocations. It can, for instance, result from microstructural barriers [87] or strain incompatibilities. The present results showed that the kinematic stress X turned out to be, both in pure fatigue and in fatigue with hold period either in creep or relaxation, the main stress component to carry the global cyclic softening effect. Whatever the loading, X decreases cyclically as the cumulated viscoplastic strain increases. Nonetheless, the influence of a hold time on the magnitude of the kinematic stress is not commonplace. Indeed, figures 5 a) to f) showed that, depending the fatigue strain range, the CF kinematic stress measured at the end of the first hold period can be either higher, almost equal or lower than the pure fatigue one. Additionaly, in the case of relaxation tests, the kinematic stress was found to be lower than the pure fatigue one for both $\Delta\epsilon_{fat} = 0.6\%$ and 0.7% (whereas for these strain ranges, the CF tests lead to higher kinematic stresses). This rather complex dependency can be correlated to another parameter linked to the strain range and to the hold time: the viscoplastic strain rate $\dot{\epsilon}^{vp}$. Figure 15.a presents the values of X measured at the first cycle for fatigue and CF tests for various strain ranges and creep amounts per cycle. In figure 16 the same values are plotted in terms of the viscoplastic strain reached at the end of the first hold period.

[Fig. 15 about here.]

[Fig. 16 about here.]

These plots highlight a rather complex dependency of the backstress X to the strain and the strain rate, and the presence of a maximum of the kinematic stress for $\dot{\epsilon}^{vp} \simeq 10^{-2}\%.s^{-1}$ suggests that at least two competing mechanisms control the value of X. The pure fatigue tests correspond to the highest values of $\dot{\epsilon}^{vp}$ ($\geq 10^{-1}\%.s^{-1}$), and for high fatigue strain amplitudes $\Delta\epsilon_{fat} = 1\%$ and 0.7% the creep rate lies between 2.10^{-3} and $5.10^{-2}\%.s^{-1}$. For these relatively high creep rates, the kinematic stress is found to be higher than the pure

fatigue one, whereas for lower creep rates, the kinematic stress is similar to the pure fatigue one (it can be noticed that for all CF tests, except that at $\Delta\epsilon_{fat} = 0.4\%$ and $\epsilon_{creep} = 0.3\%$, the first hold period corresponds to primary creep). Extremely low viscoplastic strain rates are reached in RF tests and X is found to be as small as 45MPa. The previous remarks concerning the underestimation of X for RF and CF tests do not modify these trends but would simply shift X towards higher values.
CF and RF tests differ, on the one hand, by the viscoplastic strain rate during the hold period and, on the other hand, by the nature of the stress/strain redistribution between crystallographic orientations. The following exploratory explanation could be put forward: when a creep hold is applied at high fatigue strain range, $\dot{\epsilon}^{vp}$ is high and an increase of intergranular kinematic stress takes place (the grains deform quickly and accommodation processes have no time to take place). When the viscoplastic strain rate decreases, even though strain incompatibilities may still exist, the sources of intergranular backstress can be partly accommodated by viscoplastic or time-assisted processes. Additionally, at these low strain rates, intragranular sources of backstress may also be more seldom. Indeed, dislocation pile-ups at the boundaries can vanish due to climb or cross-slip processes. These competing mechanisms highlights the difficulties inherent to the comparison of relaxation and creep tests. Whereas relaxation tests are often used to reach very low strain rates and extrapolate creep results [88], it appears that the various mechanisms responsible for backstresses may influence it in different proportions depending the type of loading. Such a complex dependency of the backstress to strain rates may be one possible reason for the unusual secondary increase of the creep rate observed [28,89].
In addition figures 15.b and .c present the same plot for $\epsilon^{vp}_{cum} = 1$ and $\epsilon^{vp}_{cum} = 10$ respectively. As mentionned above, whatever the testing conditions, the backstress X is found to decrease due to cyclic loading. For $\epsilon^{vp}_{cum} = 1$, the decrease of X is already measurable for all tests; however, the curve still presents a maximum for CF tests with high strain rates. For $\epsilon^{vp}_{cum} = 10$ the previous maximum is not visible anymore and all the X values are very low. These results show that, after cycling, the intergranular processes, evoked previously as possibly responsible for the X increase at high creep strain rates, play a very minor role, since no increase of X is measurable anymore. This is compatible with the TEM observations. As evoked in the first part [1], these examinations showed that the decrease of the kinematic stress can be related to the microstructural coarsening [2–5,46](annihilation of numerous subboundaries of the initial very fine martensitic structure [9]) observed after fatigue or RF tests. Figure 17 presents the as-received microstructure, the one observed after a pure-fatigue test and the one resulting from a RF test. It can be noticed that the numerous laths and subgrains of the as-received microstructure disappeared after cycling and led to coarse and rather equiaxed blocks. Detailed in [46,47], the mechanism proposed to account for this subboundaries vanishing is based on the annihilation of subboundary dislocations and mobile dislocations gliding thanks to the imposed plastic strain. Generally speaking,

boundary annihilation or recombination are often discussed for creep loadings [89–95]. In the present case this simple microstructural mechanism was introduced in a Hall-Petch formulation of the kinematic stress using very simple homogeneization schemes (namely Sachs and Taylor ones [96–101]). This very simple model gave encouraging results but was unable to account for the strain rate sensitivity, the viscous behaviour, the intergranular stresses variation or the slight decrease of the isotropic stress noticed in the present study.
Henceforth, a more elaborated self-consistent homogenization scheme [51,100,102] is under development to better take into account intergranular phenomena, crystalline orientation, viscosity and microstructural heterogeneities. Nevertheless, even the use of a more elaborated scale transition scheme is not sufficient to account for phenomena such as the initial latency observed in pure fatigue tests (the stress does not decrease during the first cycles, and even sometimes increases). Additional mechanisms competing with the proposed subboundaries vanishing should be taken into account. Some possibilities could be, for example, an initial hardening due to dislocation multiplication during the first cycles (numerous sources, like Scolopendra sources [103], grain boundaries ledges..., could be responsible for such a phenomenon). Or, as noticed by Meyers [55], for very fine microstructures, the first straining stages may result in the formation of a hard layer (very concentrated dislocations trapped together) around the boundaries, that may compete with the softening mechanism of microstructural coarsening. Additionally, for very long hold times, the possible coarsening of precipitates should be taken into account [42,43].

[Fig. 17 about here.]

5 Conclusions

The present paper was concerned with the cyclic viscoplastic behaviour of martensitic steels and particularly studied the influence of hold times either in creep or relaxation around 823K. The hold of either stress or strain at peak tensile stress enabled to reach large ranges of viscoplastic strains and strain rates, and to highlight the existence of a non negligible negative mean stress in CF tests. The enhanced partitioning method proposed in the first part is used to study the variations of the kinematic, isotropic and viscous parts of the cyclic stress. The following conclusions can be drawn from the previous results :

(1) For high fatigue strain ranges, the stress range lies on a single “master curve” whatever the applied creep strain, which is not true for lower fatigue strains.
(2) The isotropic stress is found to be generally insensitive to the presence

of a hold time.

(3) Whereas for pure fatigue loadings, the viscous stress σ_v supported up to one third of the total stress (for the high strain ranges, the partition was approximately $X = R = \sigma_v = \frac{1}{3}\frac{\Delta\sigma}{2}$), it decreases drastically (it decreases by up to $130MPa$ in $20s$) when a hold either in creep or relaxation is applied. This expected effect is due to the low strain rates observed during these hold periods. Activation volumes of primary creep and fatigue straining respectively close to $230b^3$ and $26b^3$ were obtained, which confirms the fact that viscous phenomena occur at a very small scale. Additionally these activation volumes were found to be independent on the microstructural changes occurring during cycling.

(4) As in the pure fatigue case, the cyclic softening effect is mainly carried by the decrease of the kinematic stress X. Nevertheless a non trivial effect of the hold periods on the magnitude of X (measured at the end of the first hold) was found. It turned out that, for high fatigue strains ranges ($\Delta\epsilon_{fat} \geq 0.7\%$), when a creep hold is applied, X is initially higher than the corresponding pure fatigue value, whereas, for low fatigue strain ranges ($\Delta\epsilon_{fat} < 0.5\%$) an opposite effect is found. This behaviour has been correlated to the viscoplastic strain rates, and the value of the kinematic stress seems to be driven by two competing mechanisms. On the one hand, the increase of the viscoplastic strain due to hold times leads to higher intergranular backstresses (mainly for CF tests). And on the other hand, when the viscoplastic strain rate decreases, accommodation mechanisms (climb, cross-slip,...) may reduce both inter and intragranular backstresses (mainly for RF tests). Therefore, the difficulty to extrapolate creep tests by the use of relaxation tests may come from the difference in the relative importance of the driving mechanisms linked to a strain rate effect.

(5) Another noticeable point concerns the fact that, during relaxation holds, both the kinematic and the viscous stresses decrease largely, which clearly invalidates the use of pure relaxation tests in order to evaluate the viscous stress. Additionally complementary sequential RF tests revealed that, due to a pronounced sensitivity to strain rate of the yield stress, the kinematic and isotropic stresses are generally underestimated by the direct use of the Cottrell partition scheme on RF (and also, to a lesser extent CF) hysteresis loops.

(6) Finally, widely opened cracks filled by oxide were identified as a possible cause of the strong Young's modulus increase measured in CF tests.

6 Acknowledgments

The direction of the Nuclear Energy of the CEA is acknowledged for financial support through the DDIN/SF project. The authors would like to thank I. Monnet, H. Brillet, A. Bougault and V. Rabeau for microscopic observations.

References

[1] B. Fournier, M. Sauzay, C. Caës, and M. Mottot. Analysis of the hysteresis loops of a martensitic steel. Part I : Study of the influence of strain amplitude and temperature under pure fatigue loadings using an enhanced stress partitionning method. *Materials Science & Engineering*, submitted 2006.

[2] B.G. Gieseke, C.R. Brinkman, and P.J. Maziasz. *The influence of thermal aging on the microstructure and fatigue properties of modified 9Cr-1Mo steel.* In Microstructures and mechanical properties of aging material, TMS The Minerals, Metals & Materials Society, 1993.

[3] A. Nagesha, M. Valsan, R. Kannan, K. Bhanu Sankara Rao, and S.L. Mannan. Influence of temperature on the low cycle fatigue behaviour of a modified 9Cr-1Mo ferritic steel. *International Journal of Fatigue*, 24:1285–1293, 2002.

[4] S. Kim and J.R. Weertman. Investigation of microstructural changes in a ferritic steel caused by high temperature fatigue. *Metallurgical Transactions A*, 19A:999–1007, 1988.

[5] A.F. Armas, C. Petersen, R. Schmitt, M. Avalos, and I. Alvarez-Armas. Mechanical and microstructural behaviour of isothermally and thermally fatigued ferritic/martensitic steels. *Journal of Nuclear Materials*, 307-311:509–513, 2002.

[6] A.F. Armas, C. Petersen, R. Schmitt, M. Avalos, and I. Alvarez. Cyclic instability of martensite laths in reduced activation ferritic/martensitic steels. *Journal of Nuclear Materials*, 329-333:252–256, 2004.

[7] A.F. Armas, M. Avalos, I. Alvarez-Armas, C. Petersen, and R. Schmitt. Dynamic strain ageing evidences during low cycle fatigue in ferritic-martensitic stainless-steels. *Journal of Nuclear Materials*, 258-263:1204–1208, 1998.

[8] N. Mebarki, D. Delagnes, P. Lamesle, F. Delmas, and C. Levaillant. Relationship between microstructure and mechanical properties of a 5% Cr tempered martensitic tool steel. *Materials Science & Engineering*, A387-389:171–175, 2004.

[9] G. Ebi and A.J. McEvily. Effect of processing on the high temperature low cycle fatigue properties of modified 9Cr-1Mo ferritic steel. *Fatigue Engng. Mater. Struc.*, 7:299–314, 1994.

[10] M. Yaguchi and Y. Takahashi. Ratchetting of viscoplastic material with cyclic softening, part 1 : experiments on modified 9Cr-1Mo steel. *International Journal of Plasticity*, 21:43–65, 2005.

[11] T. Kruml and J. Polak. Fatigue softening of X10CrAl124 ferritic steel. *Materials Science & Engineering*, A319-321:564–568, 2001.

[12] Z. Zhang, D. Delagnes, and G. Bernhart. Anisothermal cyclic plasticity of martensitic steels. *International Journal of Fatigue*, 24:635–648, 2002.

[13] L. Kunz and P. Lukas. Cyclic stress-strain behavior of 9Cr-1Mo steel at positive mean stress. *Materials Science & Engineering*, A319-321:555–558, 2001.

[14] R. Vasina, P. Lukas, L. Kunz, and V. Sklenicka. Interaction of high cycle fatigue and creep in 9%Cr-1Mo steel at elevated temperature. *Fatigue Fract. Engng Mater. Struct*, 18:27–35, 1995.

[15] A.A. Tavassoli, M. Mottot, I. Bretherton, and J. Wareing. Fatigue and creep-fatigue failure in wrought modified 9Cr 1Mo ferritic steel. Report AEA Technology -AEAT-0539, 1997.

[16] K. Aoto, R. Komine, F. Ueno, H. Kawasaki, and Y. Wada. Creep-fatigue evaluation of normalized and tempered modified 9Cr-1Mo. *Nuclear Engineering & Design*, 153:97–110, 1994.

[17] T. Goswami. Development of generic creep-fatigue life prediction. *Materials & Design*, 25:277–288, 2004.

[18] T. Sugiura, A. Ishikawa, T. Nakamura, and Y. Asada. Formulation of air environmental effect on creep-fatigue interaction. *Nuclear Engineering & Design*, 153:87–95, 1994.

[19] B.K. Choudhary, K. Bhanu Sankara Rao, S.L. Mannan, and B.P Kashyap. Low cycle fatigue, creep and creep-fatigue behaviour of forged thick section tube plate of 9Cr-1Mo ferritic steel. Euromat 96, Conference on materials and nuclear power., 1996.

[20] T. Gegenbach and A. Klenk. Creep, creep-fatigue crack intiation and growth in 9-12% chromium steels. *OMMI*, 3, 2004.

[21] S.R. Holdsworth. Creep-fatigue properties of high temperature turbine steels. *Materials at high temperature*, 18:261–265, 2001.

[22] S.L. Mannan and M. Valsan. High-temperature low cycle fatigue, creep-fatigue and thermomechanical fatigue of steels and their welds. *International Journal of Mechanical Sciences*, 2006.

[23] K. Taguchi, M. Ueta, K. Douzaki, M. Sukekawa, H. Koto, and Y. Asada. Creep-fatigue life prediction for modified 9Cr-1Mo steel. High temperature service and time-dependent failure, ASME, PVP conference, 1993.

[24] Y. Asada. Effect of air environment on creep-fatigue behavior of some commercial steels. High temperature service and time-dependent failure, ASME, PVP conference, 1993.

[25] S. Straub, P. Polcik, D. Henes, and W. Blum. Simulation of the long-term cyclic creep behaviour of a low alloyed ferritic chromium steel. *Materials Science & Engineering*, A234-236:1037–1040, 1997.

[26] R. Raj. Crack initiation in grain boundaries under conditions of steady-state and cyclic creep. *Transactions of the ASME*, page 122, 1976.

[27] M. Kimura, K. Yamaguchi, M. Hayakawa, K. Kobayashi, and K. Kanazawa. Microstructures of creep-fatigued 9-12% Cr ferritic heat-resisting steels. *International Journal of fatigue*, 28:300–308, 2006.

[28] J.S. Dubey, H. Chilukuru, J.K. Chakravartty, M. Schwienheer, A. Scholz, and W. Blum. Effects of cyclic deformation on subgrain evoution and creep in 9-12% cr-steels. *Materials Science & Engineering*, A406:152–159, 2005.

[29] A. Pineau. Mechanisms of creep-fatigue interactions. Advances in Fatigue Science and Technology, 1989.

[30] K. Sadananda and P. Shahinian. Creep-fatigue crack growth. in Cavities and cracks in creep and fatigue, J. Gittus, Applied science publishers LTD, 1981.

[31] R.H. Priest and E.G. Ellison. A combined deformation map-ductility exhaustion approach and creep fatigue analysis. *Materials Science & Engineering*, A49:7–17, 1981.

[32] W. Beere. Mechanism maps. in Cavities and cracks in creep and fatigue, J. Gittus, Applied science publishers LTD, 1981.

[33] P. Polcik, T. Sailer, W. Blum, S. Straub, J. Bursik, and A. Orlova. On the microstructural development of the tempered martensitic Cr-steel P 91 during long-term creep - a comparison of data. *Materials Science & Engineering*, A260:252–259, 1999.

[34] J. Pesicka, R. Kuzel, A. Dronhofer, and G. Eggeler. Long-term creep behavior of 9-12%Cr power plant steels. *Acta Materialia*, 51:4847–4862, 2003.

[35] W.B. Jones, C.R. Hills, and D.H. Polonis. Microstructural evolution of modified 9Cr-1Mo steel. *Metallurgical Transactions*, 22A:1049, 1991.

[36] P.J. Ennis, A. Zielinska-Lipiec, and A. Czyrska-Filemonowicz. Quantitative microscopy and creep strength of 9% chromium steels for advanced power stations. Parsons 2000 avanced materials for 21st century turbines and power plant. Proceedings of the fifth international Charles Parsons turbine conference, 2000.

[37] K. Kimura, K. Kushima, F. Abe, K. Suzuki, S. Kumai, and A. Satoh. Microstructural change and degradation behaviour of 9Cr-1Mo-V-Nb steel in the long term. Parsons 2000 avanced materials for 21st century turbines and power plant. Proceedings of the fifth international Charles Parsons turbine conference, 2000.

[38] P.J. Ennis and A. Czyrska-Filemonowicz. Recent advances in creep resistant steels for power plant application. *OMMI*, 1, 2002.

[39] J. Cadek, V. Sustek, and M. Pahütova. An analysis of a set of creep data for a 9Cr-1Mo-0.2V (P91 type) steel. *Materials Science & Engineering*, 5:165–168, 1998.

[40] Y. Qin, G. Götz, and W. Blum. Subgrain structure during annealing and creep of the cast martensitic Cr-steel G-X12CrMoWVNbN 10-1-1. *Materials Science & Engineering*, A341:211–215, 2003.

[41] H. Okamura, R. Ohtani, K. Saito, K. Kimura, R. Ishii, K. Fujiyama, S. Hongo, T. Iseki, and H. Uchida. Basic investigation for life assessment technology of modified 9Cr-1Mo steel. *Nuclear Engineering & Design*, 193:243–254, 1999.

[42] S. Spigarelli, E. Cerri, P. Bianchi, and E. Evangelista. Interpretation of creep behaviour of a 9Cr-Mo-Nb-V-N (T91) steel using threshold stress concept. *Materials Science and Technology*, 15:1433–1440, 1999.

[43] E. Cerri, E. Evangelista, S. Spigarelli, and P. Bianchi. Evolution of microstructure in a modified 9Cr-1Mo steel during short term creep. *Materials Science & Engineering*, A245:285–292, 1998.

[44] A. Orlova, J. Bursik, K. Kucharova, and V. Sklenicka. Microstructural development during high temperature creep of 9%Cr steel. *Materials Science & Engineering*, A245:39–48, 1998.

[45] T. Barkar and J. Agren. Creep simulation of 9-12% Cr steels using the composite model with thermodynamically calculated input. *Materials Science & Engineering*, A395:110–115, 2005.

[46] M. Sauzay, H. Brillet, I. Monnet, M. Mottot, F. Barcelo, B. Fournier, and A. Pineau. Cyclically induced softening due to low-angle boundary annihilation in a martensitic steel. *Materials Science & Engineering*, A400-401:241–244, 2005.

[47] B. Fournier, M. Sauzay, M. Mottot, H. Brillet, I. Monnet, and A. Pineau. Experimentally based modelling of cyclically induced softening in a martensitic steel at high temperature. Creep & Fracture in High Temperature Components - Design & Life Assessment Issues, Destech Publications Inc., Pennsylvania, USA, 2005.

[48] C. Gaudin and X. Feaugas. Cyclic creep process in AISI 316L stainless steel in terms of dislocation patterns and internal stresses. *Acta Materialia*, 52:3097–3110, 2004.

[49] J. Lemaitre and J-L. Chaboche. *Mechanics of Solid Materials*. Springer-Verlag, 1987.

[50] D. Zhou, J.C. Moosbrugger, Y. Jia, and D.J. Morrison. A substructure mixtures model for the cyclic plasticity of single slip oriented nicke single crystal at low plastic strain amplitudes. *International Journal of Plasticity*, 21:2344–2368, 2005.

[51] T. Hoc and S. Forest. Polycrystal modelling of IF-Ti steel under complex loading path. *International Journal of Plasticity*, 17:65–85, 2001.

[52] H.K. Kim, M.I. Choi, C.S. Chung, and D.H. Shin. Fatigue properties of ultrafine grained low carbon steel produced by equal channel angular pressing. *Materials Science & Engineering*, A340:243–250, 2003.

[53] S.R. Agnew and J.R. Weertman. Cyclic softening of ultrafine grain copper. *Materials Science & Engineering*, A244:143–153, 1998.

[54] H. Mughrabi, H.W. Höppel, and M. Kautz. Fatigue and microstructure of ultrafine-grained metals produced by severe plastic deformation. *Scripta Materialia*, 51:807–812, 2004.

[55] M.A. Meyers, A. Mishra, and D.J. Benson. Mechanical properties of nanocrystalline materials. *Progress in Materials Science*, 51:427–556, 2005.

[56] K. Sawada, K. Kimura, and F. Abe. Mechanical response of 9% cr heat-resistant martensitic steels to abrupt stress loading at high temperature. *Materials Science & Engineering*, A358:52–58, 2003.

[57] M. Yaguchi and Y. Takahashi. Ratchetting of viscoplastic material with cyclic softening, part 2 : application of constitutive models. *International Journal of Plasticity*, 21:835–860, 2005.

[58] K.D. Challenger and P.G. Vining. Substructure and back stress changes resulting from the cyclic loading of 2.25Cr-1Mo steel at 755K. *Materials Science & Engineering*, A58:257–267, 1983.

[59] A.H. Cottrell. *Dislocations and plastic flow in crystals.* Oxford University Press, 1953.

[60] J. Dickson, L. Handfield, and G. L'Esperance. Cyclic softening and thermally activated deformation of titanium and zirconium. *Materials Science & Engineering*, 64:L3–L7, 1983.

[61] J. Dickson, J. Boutin, and L. Handfield. A comparison of two simple methods for measuring cyclic internal and effective stresses. *Materials Science & Engineering*, 64:L7–L11, 1984.

[62] L. Handfield, J. Dickson, and G. L'Esperance. A comparison of cyclic deformation of two purities of zirconium. ICSMA7, Pergamon press, Canada, 1985.

[63] M. Sauzay, M. Mottot, L. Allais, M. Noblecourt, I. Monnet, and J. Perinet. Creep-fatigue behaviour of an AISI stainless steel at 550°C. *Nuclear Engineering & Design*, 232:219–236, 2004.

[64] C.Y. Jeong, S.W. Nam, and J. Ginztler. Activation processes of stress relaxation relaxation during hold time in 1Cr-Mo-V steel. *Materials Science & Engineering*, A264:188–193, 1999.

[65] X. Feaugas. Contribution à la compréhension des mecanismes de deformation plastique et d'endommagement des matériaux : un point de vue experimental. Memoire d'habilitation à diriger des recherches, 1999.

[66] W. Blum and A. Finkel. New technique for evaluating long range internal back stresses. *Acta Metallurgica*, 30:1705–1715, 1982.

[67] J.L. Martin, B. Lo Piccolo, T. Kruml, and J. Bonneville. Characterization of thermally activated dislocation mechanisms using transient tests. *Materials Science & Engineering*, A322:118–125, 2002.

[68] A. Orlova, J. Bonneville, and P. Spätig. Analogy between creep cycles and stress relaxation series for activation volume measurement. *Materials Science & Engineering*, A191:85–89, 1995.

[69] B. Lo Piccolo, P. Spätig, J.L. Martin, J. Bonneville, and T. Kruml. Characterising thermally activated dislocation mechanisms. *Materials Science & Engineering*, A309-310:251–255, 2001.

[70] B. Fournier, M. Sauzay, M. Mottot, V. Rabeau, A. Bougault, and A. Pineau. Fatigue crack initiation and propagation at high temperature in a softening martensitic steel. To be published in the proceedings of ECF16, Greece, 2006.

[71] R. L. Hecht. *Mechanisms operating during high-temperature fatigue with hold periods in two chromium ferritic steels.* PhD thesis, Northwestern University, 1992.

[72] H. Nakamura, K. Murali, K. Minakawa, and A.J. McEvily. Fatigue crack growth in ferritic steels as influenced by elevated temperature and environment. *Microstructure and Mechanical behaviour of materials*, 1:43–57, 1985.

[73] L. Mikulova and F. Schubert. Investigation of creep and creep fatigue crack growth behaviour of P92 in different atmospheres at temperatures above 500°C. ECCC creep conference, Creep & Fracture in high temperature components - Design & life assessment issues. London UK, Destech Publications Inc, 2005.

[74] G. Ward, B.S. Hockenhull, and P. Hancock. The effect of cyclic stressing on the oxidation of a low-carbon steel. *Metallurgical Transactions*, 5:1451–1455, 1974.

[75] A.P. Greeff, C.W. Louw, and H.C. Swart. The oxidation of industrial FeCrMo steel. *Corrosion Science*, 42:1725–1740, 2000.

[76] A.S. Khanna, P. Rodriguez, and J.B. Gnanamoorthy. Oxidation kinetics, breakaway oxidation, and inversion phenomenon in 9Cr-1Mo steels. *Oxidation of Metals*, 26, 1986.

[77] C. Ostwald and H.J. Grabke. Initial oxidation and chromium diffusion. I. Effects of surface working on 9-20% Cr steels. *Corrosion Science*, 46:1113–1127, 2004.

[78] W.M. Stobbs, S.B. Newcomb, and E. metcalfe. A microstructural study of the oxidation of Fe-Ni-Cr alloys. II 'Non-protective' oxide growth. *Philosophical Transactions of the Royal London Society*, A319:219–247, 1986.

[79] L. Martinelli. *Mécanismes de corrosion de l'acier T91 par l'eutectique Pb-Bi utilisé comme matériau de spallation.* PhD thesis, Université de Paris VI, 2005.

[80] J. Zurek, E. Wessel, L. Niewolak, F. Schmitz, T.U. Kern, L. Singheiser, and W.J. Quadakkers. Anomalous temperature dependance of oxidation kinetics during steam oxidation of ferritic steels in the temperature range 550-650°C. *Science*, 46:2301–2317, 2004.

[81] M. Schütze. Mechanical properties of oxide scales. *Oxidation of Metals*, 44, 1995.

[82] A. Daniélou, J. Rivat, M. Robillard, J. Stolarz, and T. Magnin. Fatigue mechanisms in an interstitial free steel : analysis through the behaviour of UHP -iron doped with C and Mn. *Materials Science & Engineering*, A319-321:550–554, 2001.

[83] K. Milicka and F. Dobes. Constant structure creep in a P91 type steel. *Engineering Mechanics*, 5:165–168, 1998.

[84] H.J. Frost and M.F. Ashby. *Deformation-mechanism maps*. Pergamon Press, 1982.

[85] P. Delobelle and C. Oytana. Experimental study of the flow rules of a 316 stainless steel at high stresses. *Nuclear Engineering & Design*, 83:333–348, 1984.

[86] S. Catalao, X. Feaugas, and P. Pilvin. Unpublished Report : CEA/DEN/CAD/DER/SESI/LCSI DO 20, 2004.

[87] J.C. Gibeling and W.D. Nix. A numerical study of long range internal stresses associated with subgrain boundaries. *Acta Metallurgica*, 28:1743–1752, 1980.

[88] M.F. Felsen and J. Tortel. Fluage sous contrainte variable. Fluage sous contrainte croissante. Fluage sous relaxation. Proceedings of the 23ème colloque de metallurgie - Fluage, Fatigue-fluage, Action de l'environnement, 1981.

[89] F. Abe. Coarsening behavior of lath and its effects on creep rates in tempered martensitic 9Cr-W steels. *Materials Science & Engineering*, A387-389:565–569, 2004.

[90] H.J. McQueen. The production and utility of recovered dislocation substructures. *Metallurgical Transactions A*, 8A:807, 1977.

[91] D. Caillard and J.L. Martin. Microstructure of aluminium during creep intermediate temperature - II. In situ study of subboundary properties. *Acta Metallurgica*, 30:791–798, 1982.

[92] W. Blum. Creep of crystalline materials : experimental basis, mechanisms and models. *Materials Science & Engineering*, A319-321:8–15, 2001.

[93] F. Abe, T. Horiuchi, M. Taneike, and K. Sawada. Stabilization of martensitic microstructure in advanced 9Cr steel during creep at high temperature. *Materials Science & Engineering*, A378:299–303, 2004.

[94] F. Abe, T. Horiuchi, M. Taneike, K. Kimura, S. Muneki, and M. Igarashi. Creep strain behavior during microstructure evolution in tempered martensitic advanced 9Cr steels. Proceedings of the 10th joint International Conference on Creep & Fracture of Engineering Materials and Structures., 2001.

[95] J.C.M. Li. Some elastic properties of an edge dislocation wall. *Acta Metallurgica*, 8, 1960.

[96] G. Sachs. *Zeitschrift Verein. Deut. Ing.*, 2:734–736, 1928.

[97] G.I. Taylor. Plastic strains in metals. *J. Inst. Metals*, 62:307–324, 1938.

[98] M. Bornert, T. Bretheau, and P. Gilormini. *Homogénéisation en mécanique des matériaux 1.* Hermes science, 2000.

[99] O.B. Pedersen. Mechanism maps for cyclic plasticity and fatigue of single phase materials. *Acta Metallurgica Materialia*, 38:1221–1239, 1990.

[100] R.A. Lebensohn, Y. Liu, and P. Ponte Castaneda. On the accuracy of the self-consistent approximation for polycristals : comparison with full-filled numerical simulations. *Acta Materialia*, 52:5347–5361, 2004.

[101] O.B. Pedersen and J.V. Carstensen. Internal stresses and dislocation dynamics in cyclic plasticity and fatigue of metals. *Materials Science & Engineering*, A285:253–264, 2000.

[102] M. Berveiller and A. Zaoui. An extension of the self-consistent scheme to plastically-flowing polycrystals. *Journal of the Mechanics and Physics of Solids*, 26:325–344, 1978.

[103] M. Janecek, F. Louchet, B. Doisneau-Cottignies, Y. Bréchet, and N. Guelton. Specific dislocation multiplication mechanisms and mechanical properties in nanoscaled multilayers : the example of pearlite. *Philosophical Magazine*, 80:1605–1619, 2000.

[104] H. De Cicco, M.I. Luppo, H. Raffaeli, J. Di Gaetano, L.M. Gribaudo, and J. Ovejero-Garcia. Creep behavior of an A286 type stainless steel. *Materials Characterization*, 55:97–105, 2005.

[105] K.K. Mani Pandey, O. Prakash, and B. Bhattacharya. Variation of activation volume with temperature for Fe, Si, and Ge. *Materials Letters*, 57:4319–4322, 2003.

List of Figures

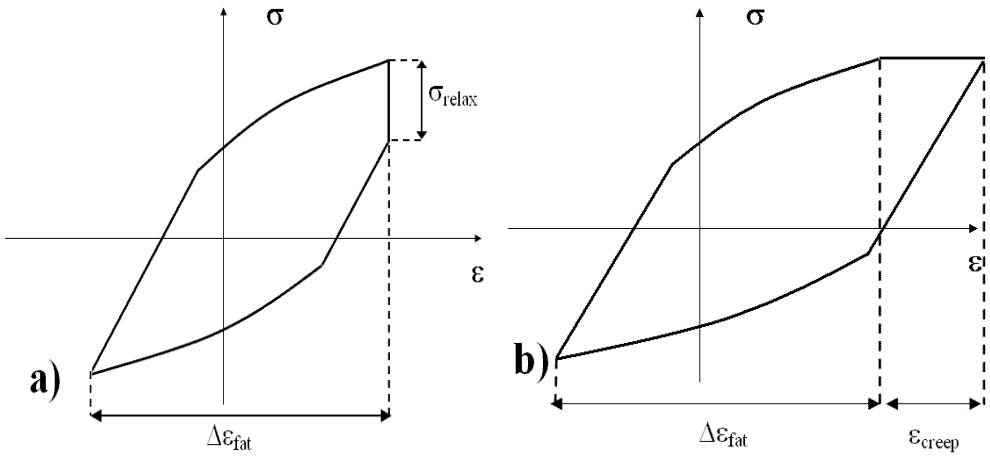

Fig. 1. Schematic shapes of the hysteresis loops of a) a RF test and b) a CF test.

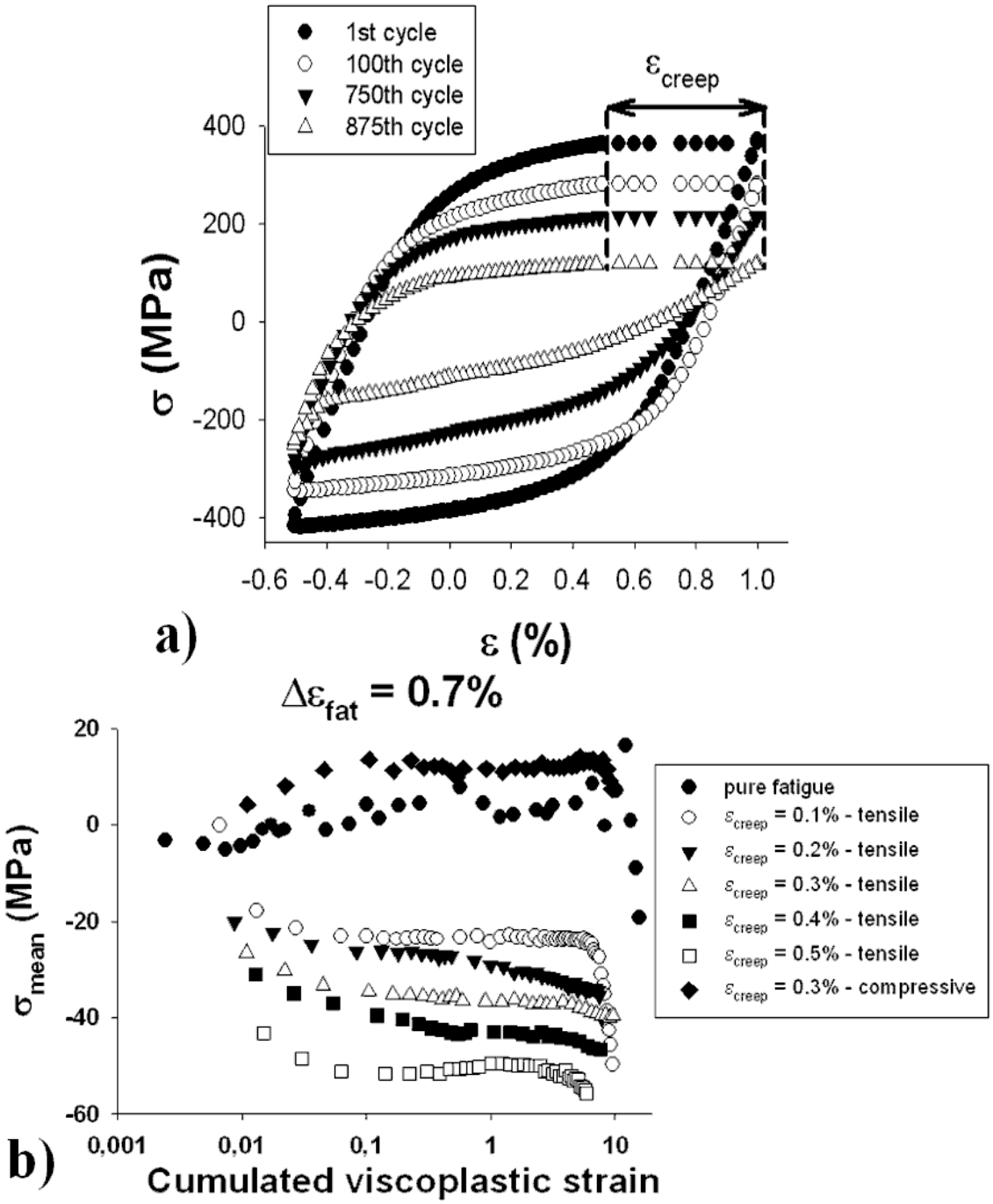

Fig. 2. a) Shapes of the hysteresis loops obtained for a CF test at $\Delta\epsilon_{fatigue} = 1\%$ and $\epsilon_{creep} = 0.5\%$, b) variation of the mean stress for pure fatigue and CF tests (with either tensile or compressive hold) at different creep strains and for $\Delta\epsilon_{fat} = 0.7\%$

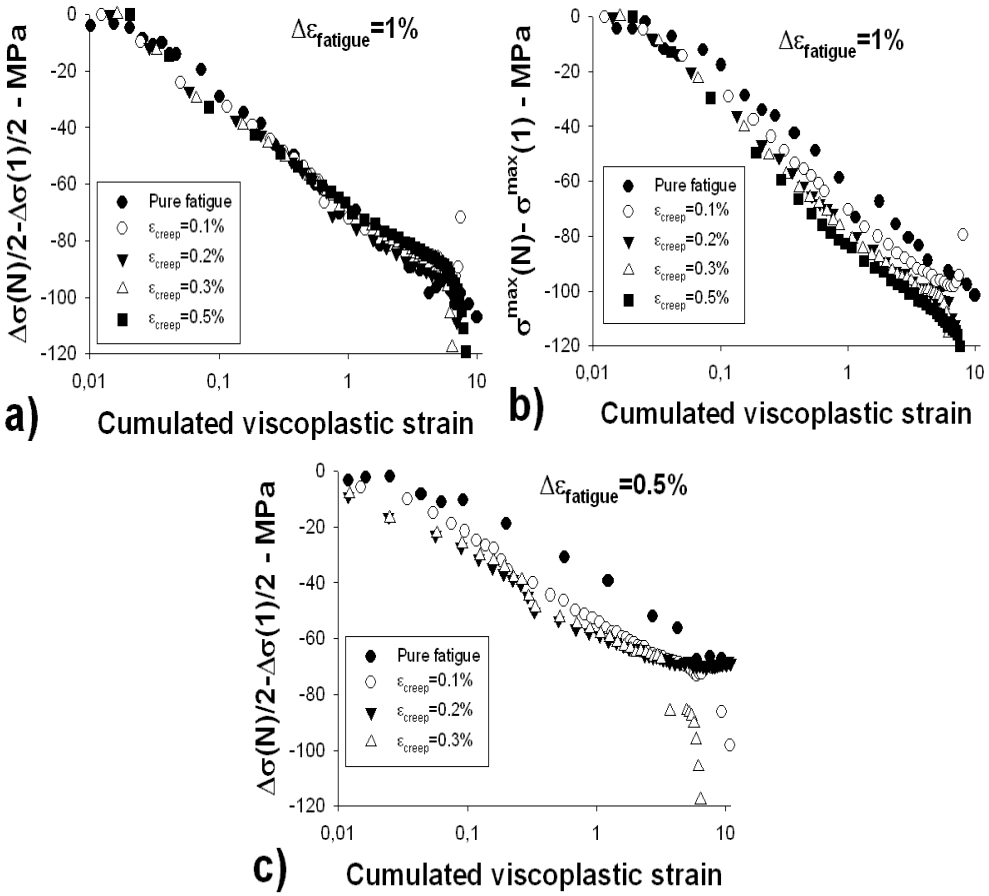

Fig. 3. variation of a) the stress amplitude $\Delta\sigma/2$ and b) of the maximum stress σ^{max} for CF tests at $\Delta\epsilon = 1\%$. c) variation of the stress amplitude for a CF test at $\Delta\epsilon = 0.5\%$.

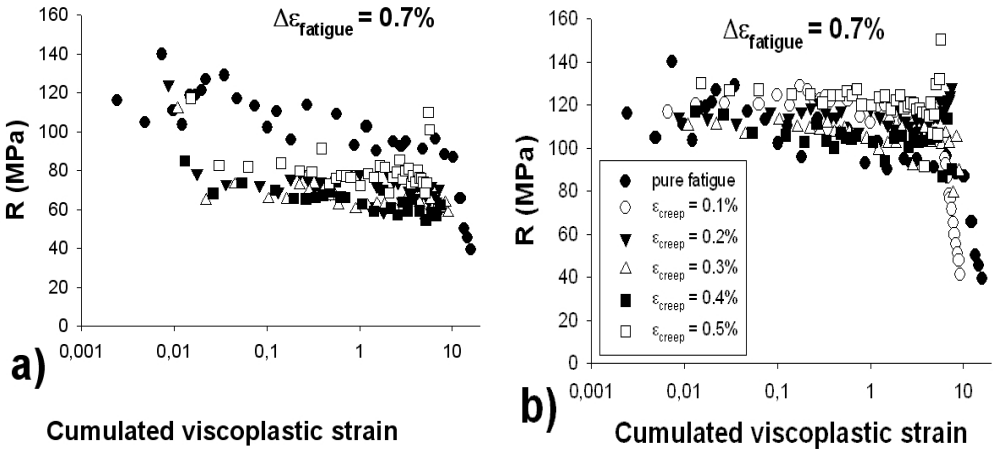

Fig. 4. variation of the isotropic stress a) in compression and b) in tension for pure fatigue and tensile CF tests at $\Delta\epsilon_{fatigue} = 0.7\%$.

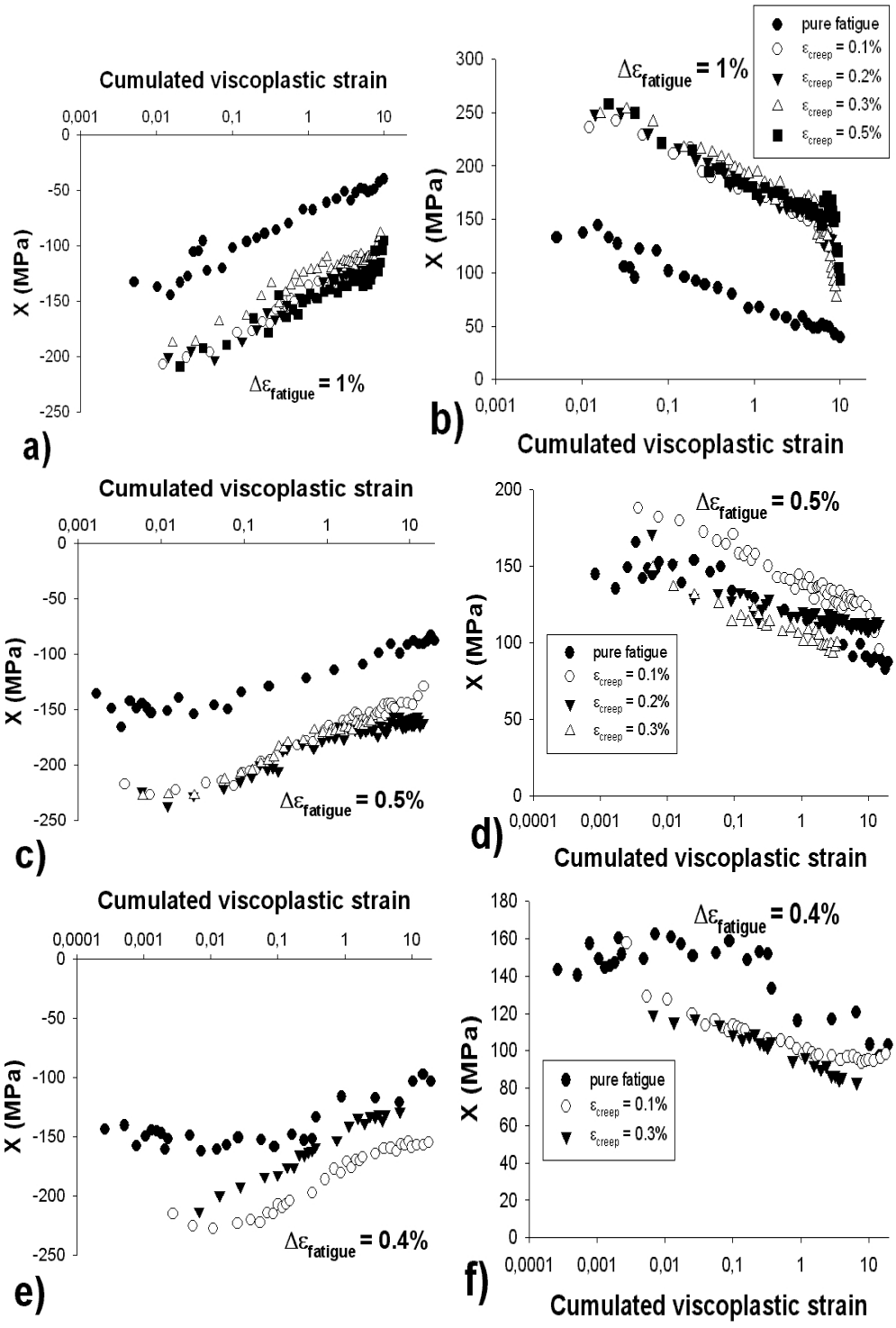

Fig. 5. variation of the kinematic stress both in compression and in tension for pure fatigue and tensile CF tests at a) and b) $\Delta\epsilon_{fatigue} = 1\%$, c) and d) $\Delta\epsilon_{fatigue} = 0.5\%$, e) and f) $\Delta\epsilon_{fatigue} = 0.4\%$.

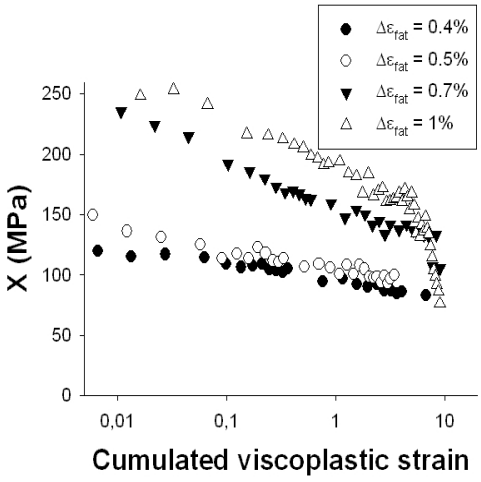

Fig. 6. variation of the kinematic stress in tension for tensile CF tests at different fatigue strains and the same creep strain $\epsilon_{creep} = 0.3\%$.

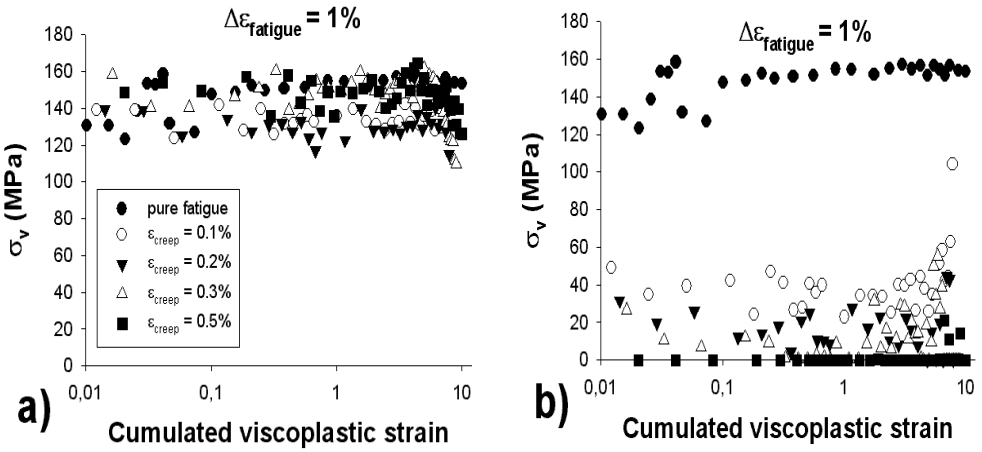

Fig. 7. variation of the viscous stress a) in compression and b) in tension for pure fatigue and tensile CF tests at $\Delta\epsilon_{fatigue} = 1\%$.

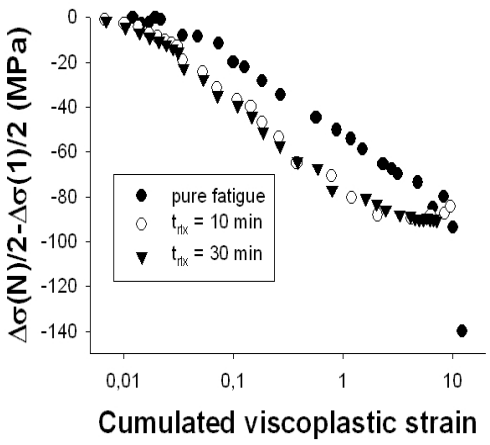

Fig. 8. variation of the stress amplitude $\Delta\sigma/2$ for RF tests at $\Delta\epsilon = 0.7\%$.

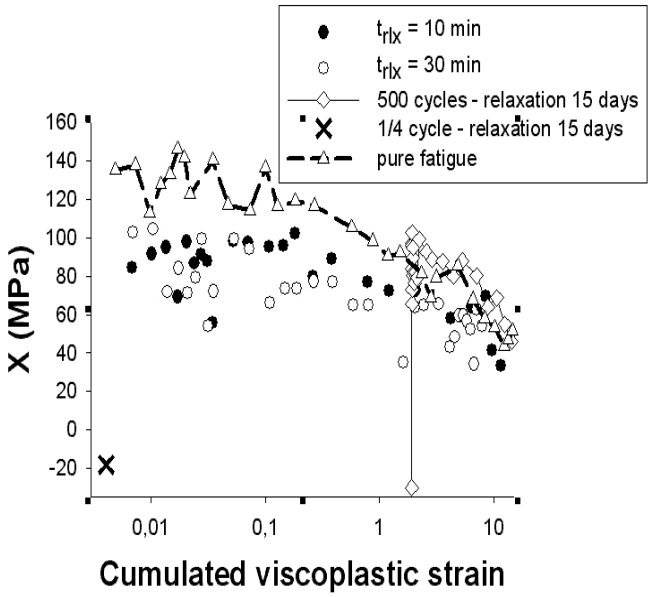

Fig. 9. variation of the kinematic stress for cyclic and sequential RF tests at $\Delta\epsilon = 0.7\%$.

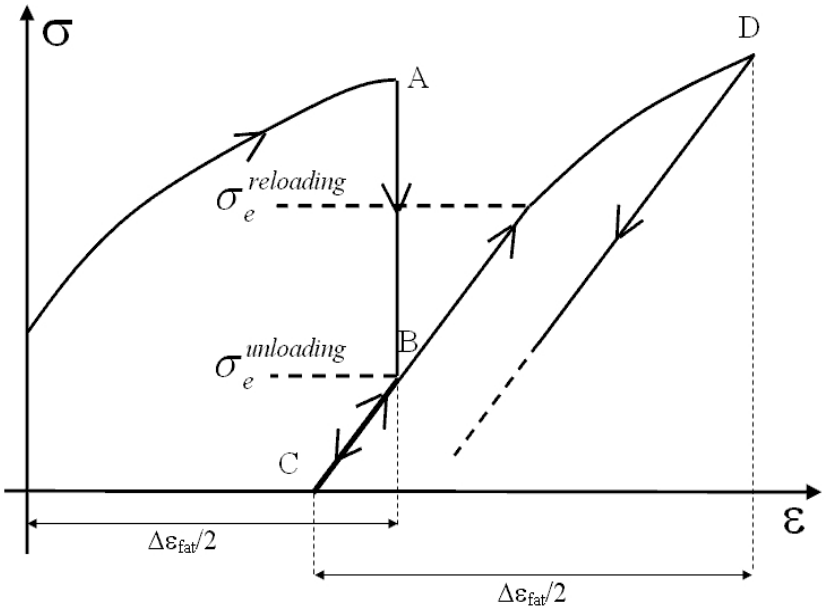

Fig. 10. Schematic illustration of the additional sequential RF tests carried out with a tensile reloading at the end of the hold period.

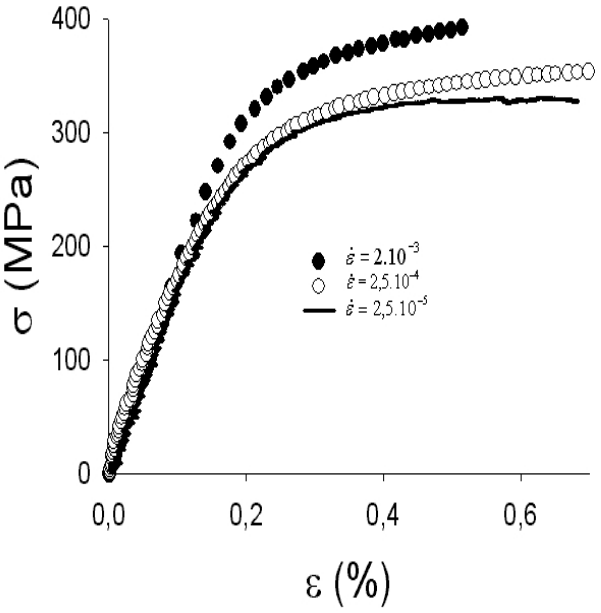

Fig. 11. Monotonic tensile curves obtained at 823K for $2.5 \times 10^{-5} \leq \dot{\epsilon} \leq 2 \times 10^{-3}$.

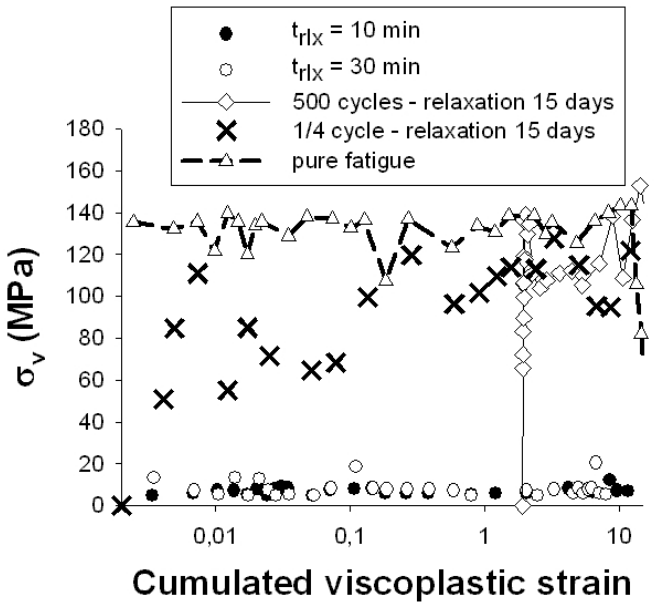

Fig. 12. variation of the viscous stress for cyclic and sequential RF tests at $\Delta\epsilon = 0.7\%$.

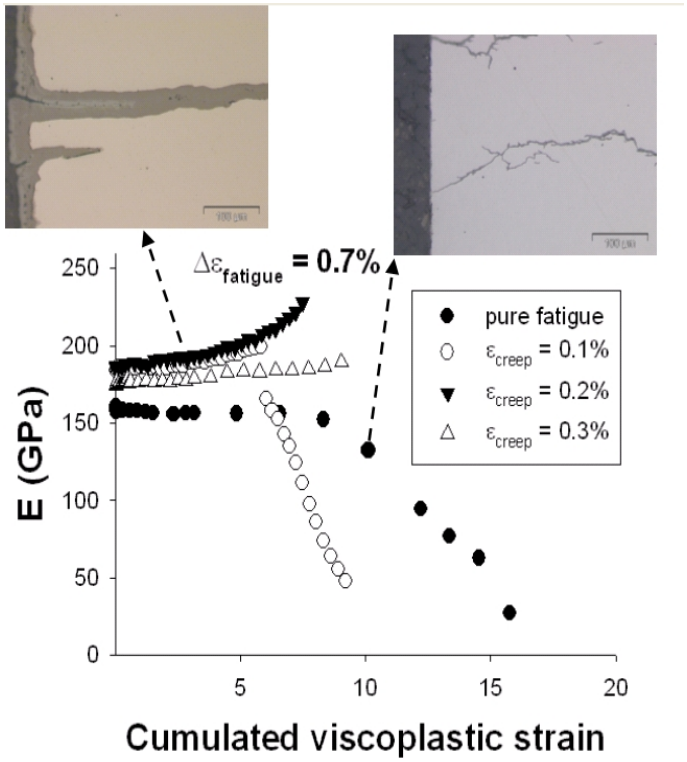

Fig. 13. variation of the effective Young modulus during CF tests at $\Delta\epsilon_{fatigue} = 0.7\%$ and observations of secondary cracks.

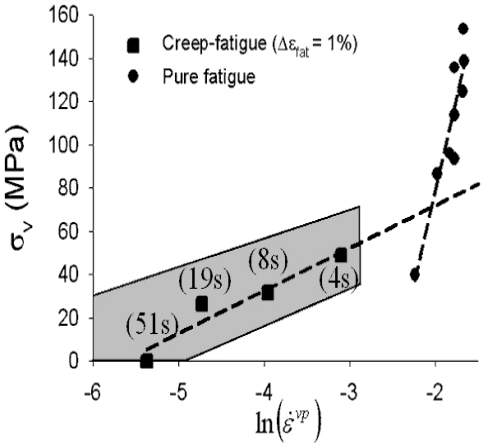

Fig. 14. Calculation of the activation volume of the viscous glide in CF tests at $\Delta\epsilon_{fatigue} = 1\%$ and pure-fatigue tests.

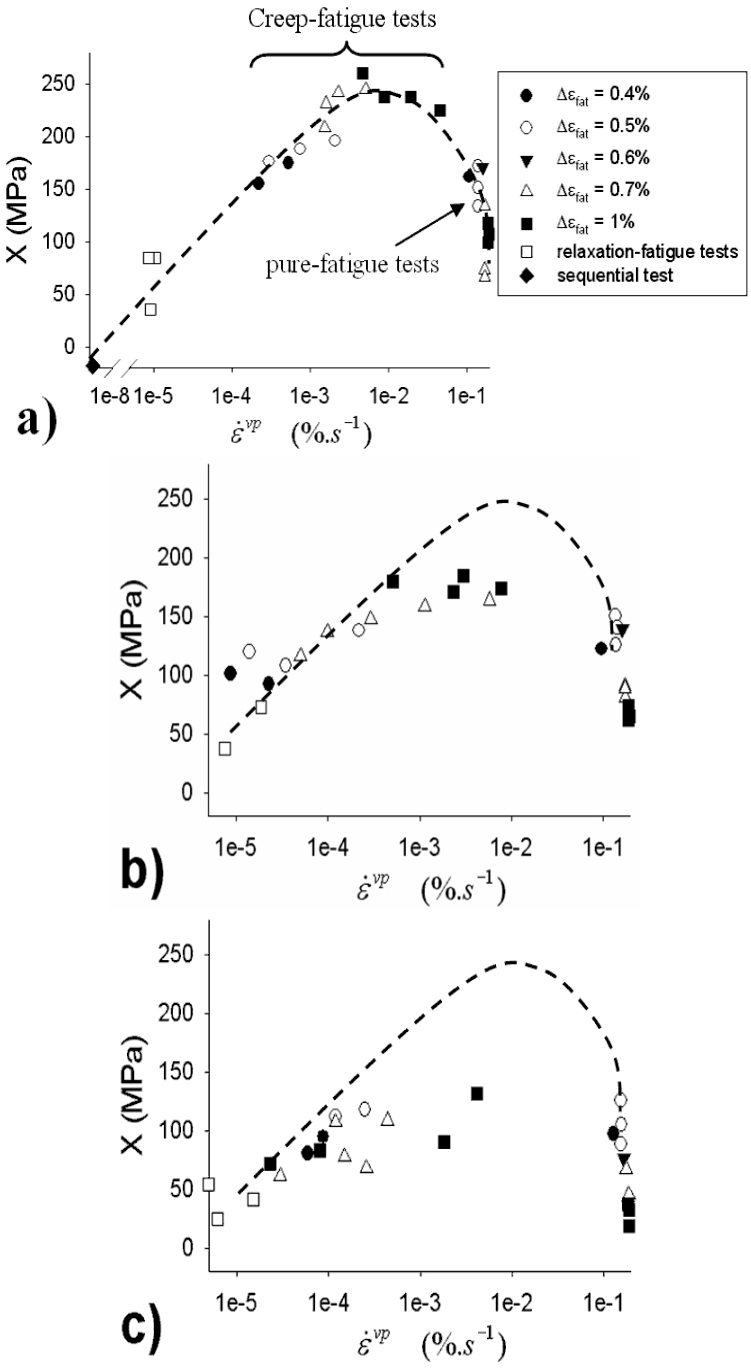

Fig. 15. Values of the kinematic stress for fatigue, CF and RF tests in terms of viscoplastic strain rate evaluated a) at the first cycle, b) for $\epsilon_{cum}^{vp} = 1$ and c) for $\epsilon_{cum}^{vp} = 10$.

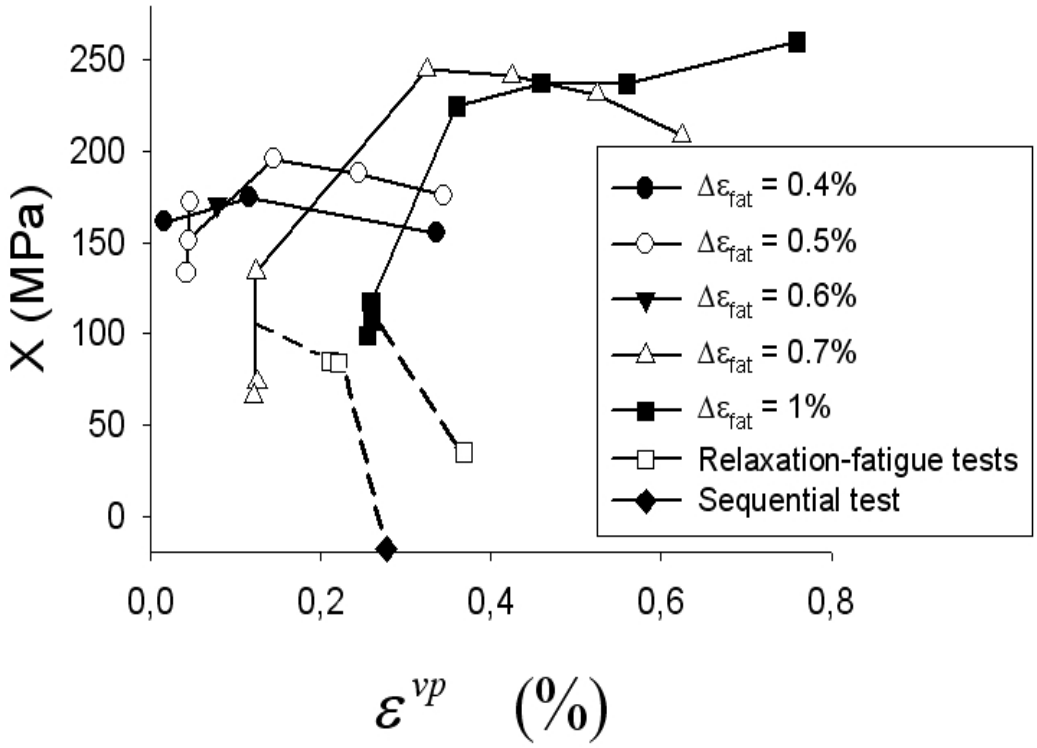

Fig. 16. Values of the kinematic stress evaluated at the first cycle for fatigue, CF and RF tests in terms of viscoplastic strain rate.

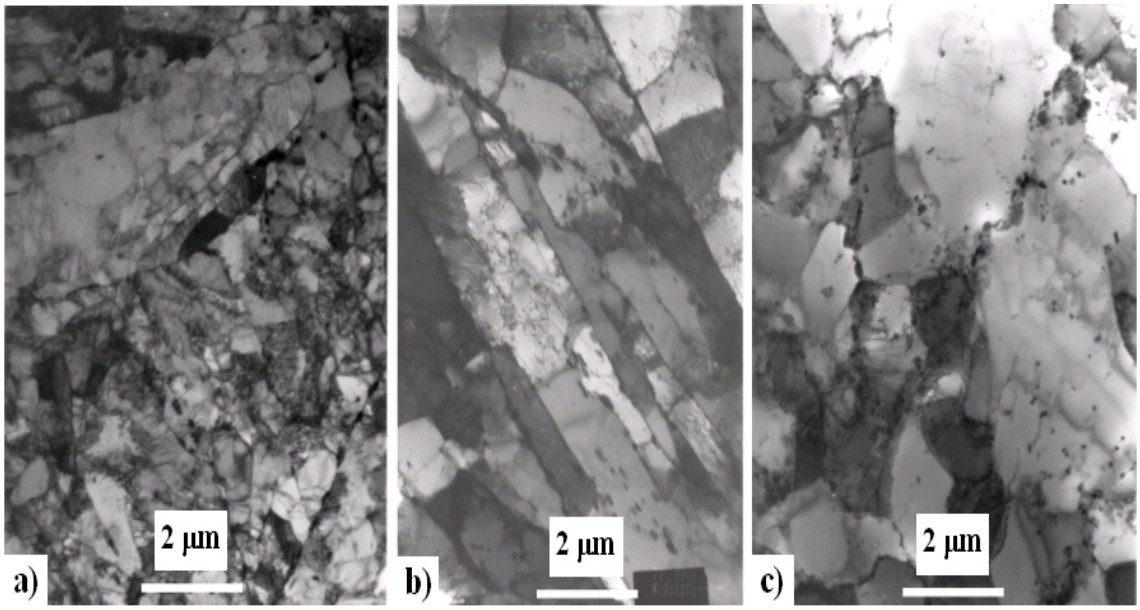

Fig. 17. TEM observations of the microstructure a) in the as-received state, b) after a pure-fatigue test ($\Delta\epsilon_{fat} = 0.7\%$ and $T = 823K$) and c) after a RF test ($\Delta\epsilon_{fat} = 0.7\%$, hold time = 90min and $T = 823K$).

List of Tables

	$\epsilon_{creep}(\%)$					
$\Delta\epsilon_{fat}(\%)$	0	0.1	0.2	0.3	0.4	0.5
0.4	4	1	0	1	0	0
0.5	3	2	1	1	0	0
0.6	4	0	0	1	0	1
0.7	3	1	1	1	1	1
1	5	2	1	1	0	1

Table 1
Number of CF tests carried at 823K for each testing condition

	hold time(min)		
$\Delta\epsilon_{fat}(\%)$	10	30	90
0.6	0	86	97
0.7	99	103	0
1	0	120	0

Table 2
Relaxed stress measured at $\frac{N_f}{2}$ of RF tests carried at 823K for each testing condition

Relaxation position	σ_e^u (MPa)	X^u (MPa)	R^u (MPa)	σ_e^r (MPa)	X^r (MPa)	R^r (MPa)
1^{st} cycle	107	-18	89	296	76.5	220
500^{th} cycle	121	-30	151	262	40.5	222

Table 3
Comparison of the stresses obtained for the sequential RF tests either with a tensile reloading (noted r) or without (noted u).

Material	T (K)	experimental technique	Activation Energy (kJ.mol^{-1})	Activation Volume (b^3)	ref
1CrMoV steel	823	relaxation	12-245	10-10^2	[64]
9Cr1Mo steel	773-873	creep	260-450	-	[19]
T91 steel	848-923	creep	680-815	-	[42]
$\alpha-$iron	293	double strain rate change	-	40-250	[82]
P91 steel	923	creep	32-400	-	[83]
P91 steel	823-923	creep	350-850	-	[39]
A286 steel	873-973	creep	-	3.5-4	[104]
$\alpha-$iron	644-866	creep indentation microhardness	-	38-115	[105]

Table 4
Some values of activation energy and activation volumes for viscous glide in 9%Cr steels and associated materials at various temperatures.